



Article

Fe₃N Nanoparticle-Encapsulated N-Doped Carbon Nanotubes on Biomass-Derived Carbon Cloth as Self-Standing Electrocatalyst for Oxygen Reduction Reaction

Yongxin Zhao ^{1,†} , Dandan Liu ^{1,†}, Yubin Tian ¹, Yuzhu Zhai ², Chaofan Tian ¹, Sen Li ¹, Tao Xing ³, Zhi Li ^{3,4} and Pengcheng Dai ^{1,*} ¹ College of New Energy, China University of Petroleum (East China), Qingdao 266580, China² College of Textile and Clothing, State Key Laboratory of Bio-Fibers and Eco-Textiles, Collaborative Innovation Center for Eco-Textiles of Shandong Province, Qingdao University, Qingdao 266101, China³ New Energy Division, National Engineering Research Center of Coal Gasification and Coal-Based Advanced Materials, Shandong Energy Group Co., Ltd., Jining 273500, China⁴ School of Materials Science and Engineering, Xi'an Jiaotong University, Xi'an 710049, China

* Correspondence: dpcapple@upc.edu.cn

† Y.Z. (Yongxin Zhao) and D.L. contributed equally to this work.

Abstract: The design and fabrication of low-cost catalysts for highly efficient oxygen reduction are of paramount importance for various renewable energy-related technologies, such as fuel cells and metal–air batteries. Herein, we report the synthesis of Fe₃N nanoparticle-encapsulated N-doped carbon nanotubes on the surface of a flexible biomass-derived carbon cloth (Fe₃N@CNTs/CC) via a simple one-step carbonization process. Taking advantage of its unique structure, Fe₃N@CNTs/CC was employed as a self-standing electrocatalyst for oxygen reduction reaction (ORR) and possessed high activity as well as excellent long-term stability and methanol resistance in alkaline media. Remarkably, Fe₃N@CNT/CC can directly play the role of both a gas diffusion layer and an electrocatalytic cathode in a zinc–air battery without additional means of catalyst loading, and it displays higher open-circuit voltage, power density, and specific capacity in comparison with a commercial Pt/C catalyst. This work is anticipated to inspire the design of cost-effective, easily prepared, and high-performance air electrodes for advanced electrochemical applications.

Keywords: Fe₃N nanoparticles; carbon nanotubes; biomass; oxygen reduction reaction; Zn–air battery



Citation: Zhao, Y.; Liu, D.; Tian, Y.; Zhai, Y.; Tian, C.; Li, S.; Xing, T.; Li, Z.; Dai, P. Fe₃N Nanoparticle-Encapsulated N-Doped Carbon Nanotubes on Biomass-Derived Carbon Cloth as Self-Standing Electrocatalyst for Oxygen Reduction Reaction. *Nanomaterials* **2023**, *13*, 2439. <https://doi.org/10.3390/nano13172439>

Academic Editor: Joohoon Kim

Received: 25 July 2023

Revised: 10 August 2023

Accepted: 17 August 2023

Published: 28 August 2023



Copyright: © 2023 by the authors. Licensee MDPI, Basel, Switzerland. This article is an open access article distributed under the terms and conditions of the Creative Commons Attribution (CC BY) license (<https://creativecommons.org/licenses/by/4.0/>).

1. Introduction

The electrochemical oxygen reduction reaction (ORR) is a critical process in air electrodes in fuel cells and metal–air batteries [1,2]. It determines the overall chemical-electrical conversion efficiency of these electrochemical devices due to the complicated 4e[−] reaction pathways, sluggish reaction kinetics, and high overpotential [3]. Platinum (Pt)-based composite materials, due to their high catalytic activity, are commonly recognized as state-of-the-art ORR electrocatalysts [3,4]. However, their large-scale applications have been severely hindered by serious drawbacks, such as scarce reserves, prohibitive costs, insufficient long-term durability, and vulnerability to methanol crossover [5,6]. Consequently, extensive efforts have been devoted to developing cost-effective electrocatalysts with competitive activity and excellent stability as alternatives to Pt-based materials.

Iron nitrides with rich N content in a carbon matrix (Fe_xN-C) containing active Fe-N-C sites [7], as a kind of newly developed non-noble metal electrocatalysts [8], present enhanced catalytic activity [9], low cost, and strong methanol tolerance [10], and have been recognized as promising alternatives to Pt-based catalysts [11,12]. For instance, Park et al. prepared a novel Fe₃N/C nanocomposite material for ORR via pyrolysis of carbon black with iron-containing precursors under an NH₃ atmosphere. The material consists of highly dispersed iron nitride nanoparticles loaded on nitrogen-doped carbon and

exhibits excellent ORR activity and direct four-electron pathway in alkaline solutions [13]. However, Fe_xN nanoparticles are thermodynamically unstable and prone to migration and coalescence during the catalysis process because of their high surface energy, resulting in an apparent decrease in activity and stability [14]. Encapsulating Fe_xN nanoparticles in the nanoshells or nanopores of a carbon matrix is one of the most promising strategies to overcome the stability issue and benefit the generation of Fe-N-C active sites [15]. Zheng et al. prepared a graphene framework with nitrogen-doped carbon nanotubes with encapsulated Fe/ Fe_3N nanoparticles through a one-step calcination strategy, which has high stability and high discharge battery voltage, close to platinum/carbon in zinc-air batteries [16]. However, most of the reported preparation strategies of carbon-encapsulated Fe_xN nanoparticles involve complex procedures, such as the pre-synthesized pyrolysis with metal-organic frameworks as precursors [3] and the polymer carbonization-acid etching route [17]. Some synthetic methods employ expensive iron and carbon precursors, such as iron phthalocyanine [18] and porphyrin [19], which increase the cost and pose challenges for large-scale synthesis. Moreover, Fe_xN -C catalysts are generally connected to a gas diffusion layer to fabricate a gas electrode with ionomers such as Nafion. Li et al. recently employed cesium salt of phosphotungstic acid as a proton conductor to replace Nafion ionomers in MEAs and explore its degradation mechanism and found that Nafion ionomers can be easily deactivated by the generated $\cdot\text{OH}$ radicals, leading to fast performance degradation [20]. By comprehensively evaluating costs, activity, and stability, the direct growth strategy of Fe_xN nanoparticles encapsulated in carbon nanomaterials on gas diffusion electrodes (i.e., carbon cloth) is highly desirable, yet few researchers have focused on this direction.

In this study, we report that Fe_3N nanoparticle-encapsulated N-doped carbon nanotubes grown on the surface of a flexible carbon cloth (denoted as $\text{Fe}_3\text{N}@\text{CNTs}/\text{CC}$) can be synthesized via simple one-step calcination of cotton cloth, one of the most commonly used biomass products. Fe_3N nanoparticles were produced during the carbonization process of the cotton cloth under an ammonia (NH_3) atmosphere and catalyzed the growth of N-doped carbon nanotubes on the generated carbon cloth, resulting in the overall fabrication of a $\text{Fe}_3\text{N}@\text{CNTs}/\text{CC}$ hierarchical structure. This hierarchical structure is capable of enlarging the surface area, promotes the exposure of active species, and gives rise to a remarkable ORR activity with a +50 mV higher half-wave potential ($E_{1/2} = 0.91$ V) than Pt/C ($E_{1/2} = 0.86$ V) in alkaline media. The long-term stability and methanol tolerance of $\text{Fe}_3\text{N}@\text{CNTs}/\text{CC}$ are also significantly improved compared to Pt/C. Meanwhile, as a flexible and free-standing electrocatalyst, $\text{Fe}_3\text{N}@\text{CNTs}/\text{CC}$ can be used directly as the air cathode in Zn-air batteries (ZIBs) and exhibits higher open-circuit voltage (1.50 V vs. 1.42 V), power density (157 mW cm^{-2} vs. 124.5 mW cm^{-2}), and specific capacity (814.9 mAh g^{-1} vs. 743.9 mAh g^{-1}) than the Pt/C based gas electrode.

2. Materials and Methods

2.1. Materials and Chemicals

Ferric chloride hexahydrate (analytical pure grade), zinc acetate dihydrate $\geq 98\%$, potassium hydroxide (analytical pure grade), concentrated sulfuric acid 98%, and ethanol 99% were purchased from Sinopsin Group Chemical Reagent Co., Ltd. (Shanghai, China) Commercial Pt/C catalyst (20 wt%) was purchased from Sigma-Aldrich (Shanghai, China), Nafion solution (5%) and Teflon dispersion (60%) were obtained from Dupont (Wilmington, DE, USA), Vulcan XC 72R (99.9%) was obtained from Johnson Matthey (London, UK), and cotton cloth (α -cellulose $> 90\%$) was purchased from Aubang Technology Co., Ltd. (Foshan, China), Deionized water was made in the laboratory.

2.2. Preparation of $\text{Fe}_3\text{N}@\text{CNT}/\text{CC}$

The cellulose cotton cloth (5 g) was washed with deionized water thrice and dried in an oven at 80 °C. Next, an impregnation solution was prepared by dissolving 2.7 g of $\text{FeCl}_3 \cdot 6\text{H}_2\text{O}$ in 5 mL of deionized water at 60 °C. The impregnation solution was then

dropped evenly onto the cellulose cotton cloth and dried at 80 °C. The impregnated cotton cloth was then annealed in a tube furnace at 1000 °C for 1 h under an NH₃ atmosphere.

2.3. Physicochemical Characterization

Material characterization: An X-ray diffractometer (XRD, χ Pert Pro, Panaco, The Netherlands) was used to characterize the phase composition of the samples. A field-emission scanning electron microscope (SEM, JSM-7500F, JEOL, Musashino, Tokyo) and a transmission electron microscope (TEM, JEM 2100F, JEOL, Musashino, Tokyo) were used to observe the surface morphology of the materials, and energy-dispersive X-ray spectroscopy (EDS) measurements were performed using a transmission electron microscope (Tecnai G20, FEI, OR, USA). X-ray photoelectron spectroscopy (XPS) was used to characterize the materials' composition, element content, and valence state. The pore structure and specific surface area of the materials were characterized by N₂ adsorption–desorption isotherms (Autosorb-iQ2, Quantachrome, FL, USA) at 77 K. The pore-size distribution plot was measured using the Barrett–Joyner–Halenda (BJH) model.

2.4. Electrochemical Measurements

Electrochemical measurements were conducted using a typical three-electrode system of a CHI760E electrochemical workstation with 0.1 M KOH as the electrolyte at 25 °C. The platinum wire and Ag/AgCl electrodes were used as the opposite and reference electrodes, respectively. The catalyst-modified glassy carbon rotating disk electrode (RDE) was used as the working electrode (0.1256 cm²). To prepare the catalyst ink, 4 mg of catalyst was mixed with 500 μ L of complex solvent (the volume ratio of ethanol/deionized water/Nafion = 9:36:5) and ultrasound for 30 min. The prepared 10 μ L catalyst ink droplet was deposited on the turntable electrode (RDE) with a catalyst load of 0.31 mg cm⁻².

During the test, cyclic voltammetry (CV) was tested in 0.1 M KOH solution saturated with O₂ or N₂ at a scan rate of 10 mV s⁻¹. Linear sweep voltammetry (LSV) was tested in 0.1 M KOH solution saturated with O₂ or N₂ at a scan rate of 5 mV s⁻¹.

The ORR kinetic currents and the number of transferred electrons were calculated using the K-L equations:

$$j^{-1} = j_k^{-1} + (j_d)^{-1} = j_k^{-1} + (B\omega^{0.5})^{-1} \quad (1)$$

$$B = 0.2nFC_0D_0^{2/3}\nu^{-1/6} \quad (2)$$

where j is the measured current density (j), j_k is the kinetic current, j_d is the diffusion-limiting current, ω is the rotating speed (revolutions per minute), n is the number of transferred electrons, F is the Faraday constant (96,485 C mol⁻¹), C_0 is the bulk concentration of O₂ (1.2×10^{-6} mol cm⁻³), D_0 is the diffusion coefficient of O₂ (1.9×10^{-5} cm² s⁻¹), and ν is the kinetic viscosity (0.01 cm² s⁻¹).

In the rotating ring-disk electrode (RRDE) test, the measured values of the ring and disk currents were used to calculate the H₂O₂ production and the number of electron transfers (n) using the following equations:

$$Y_{H_2O_2} = 2 \times (I_r/N)/(I_d + I_r/N) \times 100\% \quad (3)$$

$$n = 4I_d/(I_d + I_r/N) \quad (4)$$

where I_d denotes the disk current; I_r represents the ring current; and N is the current collection efficiency of the Pt ring with a value of 0.36 from the reduction of K₃[Fe(CN)₆]. LSV measurements via the RRDE tests were carried out at a rotating rate of 1600 rpm and a scan speed of 5 mV s⁻¹. Chronoamperometry was conducted at 0.6 V (vs. RHE) for 10,000 s (1600 rpm) in O₂-saturated 0.1 M KOH to investigate the durability of the catalyst [21].

2.5. Zn–Air Battery Tests

A Zn sheet that had been polished with sandpaper was used as the anode. Fe₃N@CNT/CC was applied as the air cathode. The aqueous electrolyte comprised 6 M KOH and 0.2 M zinc acetate. For comparison, Pt/C-based air electrode was prepared as follows: 1 mg of Pt/C catalyst, 400 μ L of anhydrous ethanol, and 10 μ L of Nafion were mixed evenly and then deposited on the commercial carbon cloth with a Pt/C loading mass of 0.82 mg cm⁻².

3. Results and Discussion

3.1. Structural and Compositional Analyses

Fe₃N@CNT/CC was prepared via a simple thermal treatment of FeCl₃-decorated cellulose cotton cloth under an NH₃ atmosphere, as illustrated in Figure 1a. The digital images of the Fe₃N@CNT/CC film in Figure 1b reveal its excellent flexibility, as it can be bent and rolled without structural deterioration. ICP and elemental analysis were performed to identify the composition ratios of the Fe₃N@CNTs/CC film. As shown in Table S1, the weight fraction of Fe, C, N, and O is 20.096%, 72.23%, 5.067%, and 2.182%, respectively. Thus, the weight fraction of the ORR active Fe₃N species was determined to be 21.8%. SEM was used to analyze the morphology of Fe₃N@CNT/CC. It is observed that the fiber-braided structure of the cotton cloth is well retained during the carbonization process (Figure 1c). Carbon nanotubes are generated and connected to the fibers (Figure 1d) with a diameter of \sim 100 nm (Figure 1e). Shiny nanoparticles are observed to be encapsulated within the carbon nanotubes (Figure 1e). As shown in the TEM and STEM images (Figures 1f and S1), the diameters of Fe₃N nanoparticles are in the range of 30–80 nm. The lattice spacing of the nanoparticles is 0.206 nm (Figure 1g), corresponding to the (-1-11) crystal plane of Fe₃N [21,22]. Additionally, clear lattice fringes are observed outside the nanoparticles with a lattice spacing of 0.34 nm, corresponding to the (002) crystal plane of graphite carbon. The elemental mapping reveals that C and N are evenly distributed throughout the carbon nanotubes, forming N-doped carbon nanotubes. In contrast, Fe is only distributed in the cores of the carbon nanotubes (Figure 1h), indicating Fe₃N nanoparticles are encapsulated in the carbon nanotubes. In this way, Fe₃N nanoparticles are trapped in the nanocavity of carbon nanotubes, preventing catalyst agglomeration [23].

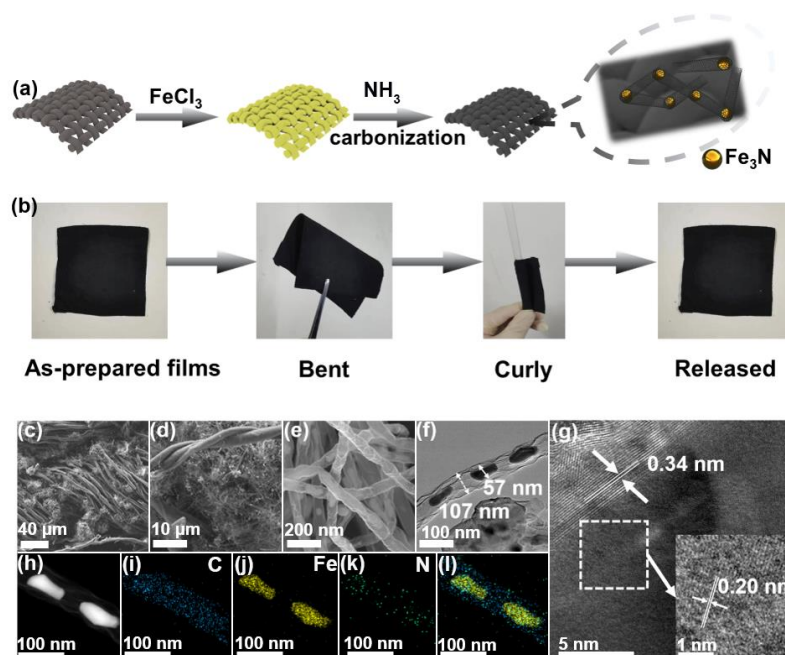


Figure 1. (a) Illustration of the synthetic process of Fe₃N@CNT/CC. (b) Digital photos showing the flexibility of Fe₃N@CNT/CC. (c,d) SEM images, (e) STEM image, (f) TEM image, (g) HRTEM image, and (h–l) TEM selective area and its corresponding EDS elemental mappings of Fe₃N@CNT/CC.

X-ray diffraction (XRD) spectrum was recorded to analyze the crystallinity of the obtained Fe₃N@CNT/CC film (Figure 2a). The diffraction peaks at 38.2°, 41.1°, 43.6°, 57.3°, 69°, and 76.5° correspond to the (110), (002), (-1-11), (-1-12), (300), and (-1-13) crystal planes of Fe₃N, respectively [3]. The diffraction peak at 26.4° corresponds to the (002) facet of graphite carbon [3], consistent with the HRTEM results. The average crystallite size calculated based on the Scherrer formula is 52 nm, consistent with the STEM result in Figure S1. Figure 2b depicts the Raman spectrogram analysis of the Fe₃N@CNT/CC film, which exhibits two distinct peaks at 1344 cm⁻¹ and 1574 cm⁻¹, corresponding to the typical D and G bands of carbon materials [24]. The ratio of I_D/I_G indicates the degree of defect of the carbon material [25]. The I_D/I_G value of Fe₃N@CNT/CC was determined to be about 0.89, which suggests that less defective or amorphous carbon exists in the as-prepared product. The nitrogen adsorption and desorption isotherm reveal that Fe₃N@CNT/CC possesses a specific surface area of 337.7 m²·g⁻¹ (Figure 2c). The pore volume is mainly contributed by micropores, while a certain amount of mesopores also exist with an average size of 4 nm (Figure 2d). The high surface area and pore volume can make the catalytically active sites accessible and ensure fast mass transport efficiency, which enables the catalyst to have significant advantages during electrocatalytic reactions [26,27].

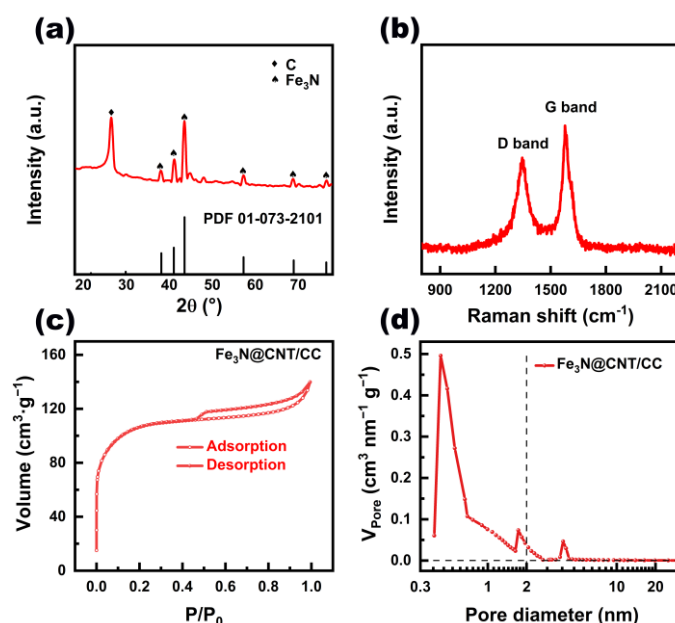


Figure 2. (a) XRD pattern, (b) Raman spectrum, (c) nitrogen adsorption and desorption isotherm, and (d) pore-size distribution of Fe₃N@CNT/CC.

XPS characterizations were further performed to investigate the elements' specific contents (Table S2) and chemical states on the surface of Fe₃N@CNT/CC. The XPS survey spectrum (Figure 3a) reveals the presence of C, N, Fe, and O. The molar fraction of Fe, C, N, and O determined by XPS is 47.1%, 17.9%, 23.7%, and 11.3%. Compared to the ICP and elemental analysis results, the contents of Fe, N, and O determined by XPS are much higher, and the carbon content is lower. This result further proves that Fe₃N nanoparticles and N-doped carbon nanotubes are grown on the surface of the carbon cloth. In the C 1s spectrum (Figure 3b), the peaks at 284.8 eV, 285.5 eV, and 287.8 eV correspond to C-C, C-N, and C-O signals, respectively [28]. The N 1s (Figure 3c) spectrum is divided into four peaks, including pyridinic nitrogen (398.2 eV), Fe-N_x (399.4 eV), pyrrolic nitrogen (401 eV), and graphite nitrogen (402.1 eV) [29]. The ratio of graphitic N, pyrrolic N, pyridinic N, and Fe-N_x is 37.6%: 26.3%: 14.6%: 21.5%. The peak corresponding to the Fe-N bond can be observed at 707.8 eV [30]. The Fe 2p spectrum exhibits a peak ascribed to Fe₃N at the binding energy of 707.8 eV (Figure 3d) [3]. The peaks at the binding energies of 710.7/724.3 and 712.7/726.2 eV originated from Fe²⁺-N/O and Fe³⁺-N/O due to the surface

oxidation of the sample [31]. The existence of C-N in the C 1s spectrum, Fe-N_x in the N 1s spectrum, and the Fe-N bond in the Fe 2p spectrum verifies the formation of Fe-N-C sites, which have been proven to be efficient ORR active sites [32]. Meanwhile, the graphitized N-doped carbon promotes the electron transfer process, further improving the electrical conductivity of the sample [3].

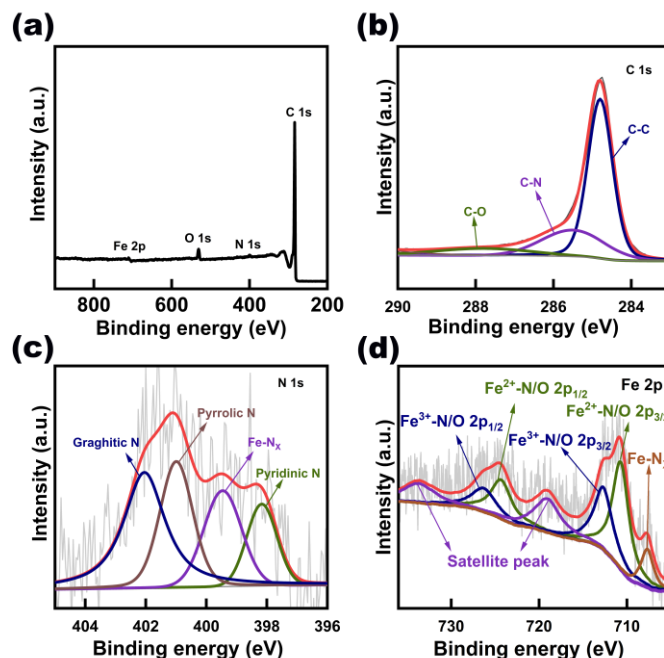


Figure 3. (a) XPS survey spectrum, (b) high-resolution C 1s, (c) high-resolution N 1s, and (d) high-resolution Fe 2p spectrum of Fe₃N@CNT/CC.

3.2. Electrocatalytic Activities of Fe₃N@CNT/CC for ORR

The ORR performances of Fe₃N@CNT/CC were compared with those of commercial Pt/C (Figure 4). Fe₃N@CNT/CC demonstrated no ORR peaks in the N₂-saturated electrolyte, while a distinguished reduction peak for ORR appeared when the electrolyte was saturated with O₂ (Figure 4a). The peak potentials corresponding to Fe₃N@CNT/CC were 0.91 V, which was 60 mV more positive than that of the corresponding 20% Pt/C (0.85 V) (Figures 4a and S2). The LSV curve of Fe₃N@CNT/CC (Figure 4b) shows an onset potential of 1.0 V, a half-wave potential of 0.91 V, and a limit current density of 5.6 mA·cm⁻¹. In contrast, the initial potential (0.9 V), half-wave potential (0.86 V), and limit current (5 mA·cm⁻¹) of the Pt/C catalyst were significantly worse than those of Fe₃N@CNT/CC. The corresponding Tafel slope of Fe₃N@CNT/CC (Figure 4c) was 78 mV·dec⁻¹, which was lower than that of Pt/C (88 mV·dec⁻¹), indicating that Fe₃N@CNT/CC has a faster catalytic kinetic process [3].

The ORR reactions have two types of electron transfer processes: 2e⁻ transfer process and 4e⁻ transfer process. In the 2e⁻ transfer process, oxygen reacts to produce H₂O₂ through the catalytic process [33]. The reaction rate of this process is slow, which is not suitable for application in zinc–air batteries [34]. Moreover, the generated H₂O₂ can cause damage to the catalyst and battery components [35,36]. The catalytic product of the 4e⁻ transfer process is H₂O, making it the required catalytic path for the ORR catalytic reaction [37]. The number of transferred electrons (n) in the catalytic reactions was obtained based on the Koutecký–Levich (K-L) calculation of the LSV curves at different speeds (Figure 4d). As shown in Figure 4e, the average number of transferred electrons of Fe₃N@CNT/CC was determined to be 3.99, which is close to the theoretical value of 4 and comparable to that of Pt/C. In addition, rotating ring-disk electrode (RRDE) measurements were conducted to explore the ORR pathway of Fe₃N@CNT/CC (Figure S3). The H₂O₂

yield of $\text{Fe}_3\text{N@CNT/CC}$ was found to be only 0.14%–0.01% from 0.2 V to 0.8 V (Figure 4f), further proving the $4e^-$ transfer process.

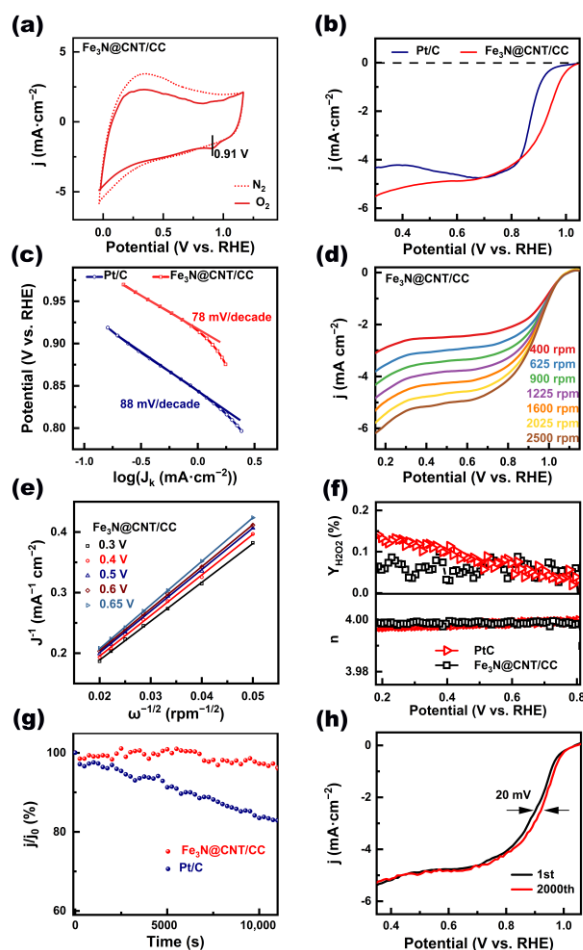


Figure 4. (a) CV curves of $\text{Fe}_3\text{N@CNT/CC}$ in N_2 (dotted line)- and O_2 (solid line)-saturated 0.1 M KOH electrolytes with a scan rate of $10 \text{ mV}\cdot\text{s}^{-1}$; (b) LSV curves of $\text{Fe}_3\text{N@CNT/CC}$ and Pt/C, (c) corresponding Tafel plots and slopes; (d) LSV curves of $\text{Fe}_3\text{N@CNT/CC}$ at different speeds; (e) K-L plot of $\text{Fe}_3\text{N@CNT/CC}$; (f) electron transfer number and H_2O_2 yield of $\text{Fe}_3\text{N@CNT/CC}$ and Pt/C; (g) long-term stability test of $\text{Fe}_3\text{N@CNT/CC}$ and Pt/C; and (h) durability measurement of $\text{Fe}_3\text{N@CNT/CC}$.

Subsequently, the stability of the $\text{Fe}_3\text{N@CNT/CC}$ and Pt/C catalysts was assessed using timed amperometry at 0.8 V (vs. RHE). The current retention of $\text{Fe}_3\text{N@CNT/CC}$ decreased by 2.75% during the test at 10,000 s, whereas that of the Pt/C catalyst decreased by 16.5% (Figure 4g). It was observed that $\text{Fe}_3\text{N@CNT/CC}$ is more stable during the reaction. Figure 4h depicts the durability test of $\text{Fe}_3\text{N@CNT/CC}$ after 2000 CV cycle curves. It can be observed that the half-wave potential value of the catalyst only decreased by 20 mV after 2000 accelerated aging experiments, indicating its excellent stability as well. Methanol resistance is another essential index in ORR. It can be seen from Figure S3 that when methanol was added to the electrolyte, the current value of $\text{Fe}_3\text{N@CNT/CC}$ decreased by 5%, whereas the current density of Pt/C decreased by 35% (Figure S4), which suggests that $\text{Fe}_3\text{N@CNT/CC}$ exhibits outstanding resistance to methanol.

3.3. Application of $\text{Fe}_3\text{N@CNT/CC}$ Catalyst in ZAB

To further evaluate the practical application of $\text{Fe}_3\text{N@CNT/CC}$, it is essential to assemble it as the air cathode in a ZAB, as illustrated in Figure 5a. The open-circuit voltage of the carbon cloth composed of $\text{Fe}_3\text{N@CNT/CC}$ is approximately 1.5 V (Figure 5b), which

is higher than that of Pt/C (1.43 V). As shown in Figure 5c, Fe₃N@CNT/CC can supply a higher voltage at the same current density than Pt/C. The peak discharge power density of the ZAB with Fe₃N@CNT/CC as the air cathode is 157 mW cm⁻² at the current density of 300 mA cm⁻² (Figure 5c,d), which is higher than that of the Pt/C catalyst (124.5 mW cm⁻²). Figure 5e illustrates the constant current discharge test of the battery at a current density of 10 mA cm⁻². The specific capacity of the Fe₃N@CNT/CC-based ZAB is 814.9 mAh g⁻¹, also higher than that of the Pt/C catalyst (737.9 mAh g⁻¹). In addition, Figure 5f depicts the cycling stability of the Fe₃N@CNT/CC-based ZAB. The voltage range does not widen during the 100 h charge–discharge cycle, indicating the catalyst has excellent stability.

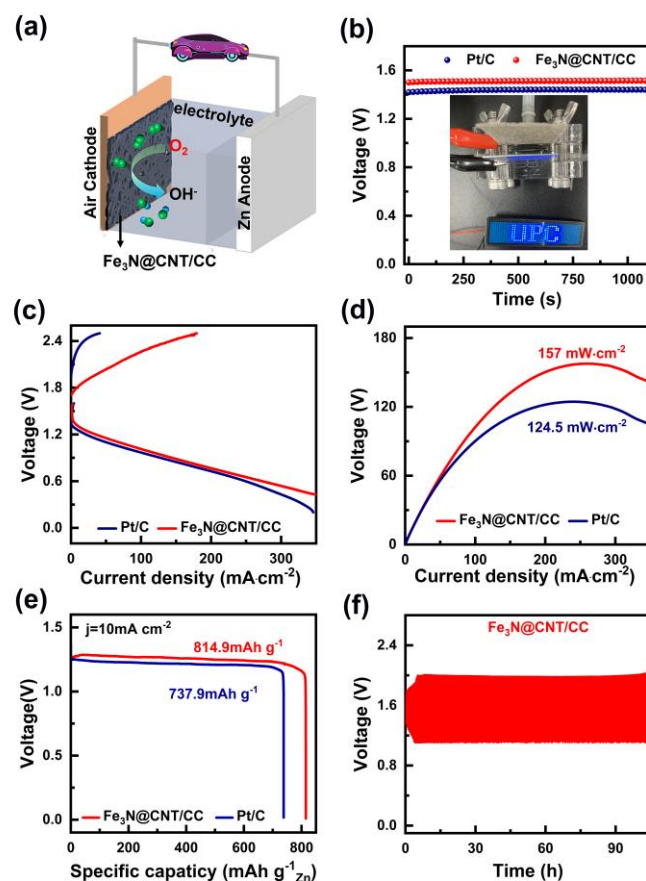


Figure 5. (a) Schematic of the as-assembled zinc–air battery, (b) open-circuit voltage, (c) polarization curves, (d) power density curves of the ZABs assembled with Fe₃N@CNT/CC and Pt/C, (e) the discharge specific capacity curves of the ZABs with Fe₃N@CNT/CC and Pt/C at a current density of 10 mA cm⁻², and (f) the cycling stability of the Fe₃N@CNT/CC-based ZAB.

4. Conclusions

In this work, Fe₃N nanoparticle-encapsulated N-doped carbon nanotubes grown on the surface of a flexible carbon cloth were synthesized via simple one-step calcination of the cotton cloth. The structural features and ORR performance of the as-prepared catalysts were investigated in detail. The hierarchical structure can stabilize the active sites, promotes the exposure of active species, and possesses satisfactory ORR performance, including excellent half-wave potential, higher long-term stability, and satisfactory resistance to methanol, outperforming the commercial Pt/C catalysts. Benefiting from the unique structure, Fe₃N@CNTs/CC can be used directly as a free-standing air cathode in ZABs, exhibiting higher open-circuit voltage, power density, and specific capacity than a Pt/C-based gas electrode. This work paves the way for the construction of cost-effective, easily prepared, and high-performance ORR catalysts and ZAB-based energy conversion devices.

Supplementary Materials: The following supporting information can be downloaded at <https://www.mdpi.com/article/10.3390/nano13172439/s1>. Figure S1: CV curves of the Pt/C catalyst in N₂- and O₂-saturated 0.1 M KOH electrolytes with a scan rate of 10 mV·s⁻¹. Figure S2: RRDE voltammograms of Fe₃N@CNT/CC at a rotation rate of 1600 rpm. Figure S3: The chronoamperometric curves of Fe₃N@CNT/CC and Pt/C acquired by injecting 1.0 M methanol at 100 s. Figure S4: The chronoamperometric curves of Fe₃N@CNT/CC and Pt/C acquired by injecting 1.0 M methanol at 100 s; Table S1: Proportion of element content. Table S2: Atomic percentage of C, N, O, Fe on the surface of Fe₃N@CNT/CC.

Author Contributions: Conceptualization, D.L. and P.D.; methodology, Y.T.; validation, D.L.; formal analysis, C.T.; data curation, S.L.; writing—original draft preparation, Y.Z. (Yongxin Zhao); writing—review and editing, Y.Z. (Yuzhu Zhai); visualization, Y.Z. (Yuzhu Zhai); supervision, P.D.; funding acquisition, T.X. and Z.L. All authors have read and agreed to the published version of the manuscript.

Funding: This research was funded by the National Natural Science Foundation of China (51702365), the Natural Science Foundation of Shandong Province (ZR2022MB133), the Key Research and Development Plan of Shandong Province (2019GGX102056, 2018GGX104018), and New Faculty Start-up funding in China University of Petroleum (East China) (YJ201501029).

Data Availability Statement: The data presented in this study are available upon request from the corresponding author.

Conflicts of Interest: The authors declare no conflict of interest.

References

1. Nie, Y.; Xu, X.; Wang, X.; Liu, M.; Gao, T.; Liu, B.; Li, L.; Meng, X.; Gu, P.; Zou, J. Coni alloys encapsulated in N-doped carbon nanotubes for stabilizing oxygen electrocatalysis in zinc-air battery. *Nanomaterials* **2023**, *13*, 1788. [\[CrossRef\]](#)
2. Cebollada, J.; Sebastián, D.; Lázaro, M.J.; Martínez-Huerta, M.V. Carbonized polydopamine-based nanocomposites: The effect of transition metals on the oxygen electrocatalytic activity. *Nanomaterials* **2023**, *13*, 1549. [\[CrossRef\]](#)
3. Li, T.; Li, M.; Zhang, M.; Li, X.; Liu, K.; Zhang, M.; Liu, X.; Sun, D.; Xu, L.; Zhang, Y.; et al. Immobilization of Fe₃N nanoparticles within N-doped carbon nanosheet frameworks as a high-efficiency electrocatalyst for oxygen reduction reaction in zn-air batteries. *Carbon* **2019**, *153*, 364–371. [\[CrossRef\]](#)
4. Radwan, A.; Jin, H.; Liu, B.; Chen, Z.; Wu, Q.; Zhao, X.; He, D.; Mu, S. 3D-ZIF scaffold derived carbon encapsulated iron nitride as a synergistic catalyst for ORR and zinc-air battery cathodes. *Carbon* **2021**, *171*, 368–375. [\[CrossRef\]](#)
5. Yu, X.; Ye, S. Recent advances in activity and durability enhancement of pt/c catalytic cathode in pemfc: Part ii: Degradation mechanism and durability enhancement of carbon supported platinum catalyst. *J. Power Sources* **2007**, *172*, 133–144. [\[CrossRef\]](#)
6. Xue, N.; Liu, J.; Wang, P.; Wang, C.; Li, S.; Zhu, H.; Yin, J. Scalable synthesis of Fe₃N nanoparticles within N-doped carbon frameworks as efficient electrocatalysts for oxygen reduction reaction. *J. Colloid Interface Sci.* **2020**, *580*, 460–469. [\[CrossRef\]](#)
7. Dong, Q.; Li, G.; Liu, F.; Ren, J.; Wang, H.; Wang, R. Cu nanoclusters activating ultrafine Fe₃N nanoparticles via the mott-schottky effect for rechargeable zinc-air batteries. *Appl. Catal. B Environ.* **2023**, *326*, 122415. [\[CrossRef\]](#)
8. Noh, W.Y.; Mun, J.; Lee, Y.; Kim, E.M.; Kim, Y.K.; Kim, K.Y.; Jeong, H.Y.; Lee, J.H.; Song, H.-K.; Lee, G.; et al. Molecularly engineered carbon platform to anchor edge-hosted single-atomic M-N/C (M = Fe, Co, Ni, Cu) electrocatalysts of outstanding durability. *ACS Catal.* **2022**, *12*, 7994–8006. [\[CrossRef\]](#)
9. Yang, G.; Zhu, J.; Yuan, P.; Hu, Y.; Qu, G.; Lu, B.-A.; Xue, X.; Yin, H.; Cheng, W.; Cheng, J.; et al. Regulating fe-spin state by atomically dispersed Mn-N in Fe-N-C catalysts with high oxygen reduction activity. *Nat. Commun.* **2021**, *12*, 1734. [\[CrossRef\]](#)
10. Mazzucato, M.; Daniel, G.; Mehmood, A.; Kosmala, T.; Granozzi, G.; Kucernak, A.; Durante, C. Effects of the induced micro- and meso-porosity on the single site density and turn over frequency of Fe-N-C carbon electrodes for the oxygen reduction reaction. *Appl. Catal. B Environ.* **2021**, *291*, 120068. [\[CrossRef\]](#)
11. Yang, W.; Chen, L.; Liu, X.; Jia, J.; Guo, S. A new method for developing defect-rich graphene nanoribbons/onion-like carbon@co nanoparticles hybrid materials as an excellent catalyst for oxygen reactions. *Nanoscale* **2017**, *9*, 1738–1744. [\[CrossRef\]](#) [\[PubMed\]](#)
12. Xiao, J.; Xu, Y.; Xia, Y.; Xi, J.; Wang, S. Ultra-small Fe₂N nanocrystals embedded into mesoporous nitroge N-doped graphitic carbon spheres as a highly active, stable, and methanol-tolerant electrocatalyst for the oxygen reduction reaction. *Nano Energy* **2016**, *24*, 121–129. [\[CrossRef\]](#)
13. Park, M.J.; Lee, J.H.; Hembram, K.P.S.S.; Lee, K.-R.; Han, S.S.; Yoon, C.W.; Nam, S.-W.; Kim, J.Y. Oxygen reduction electrocatalysts based on coupled iron nitride nanoparticles with nitrogen-doped carbon. *Catalysts* **2016**, *6*, 86. [\[CrossRef\]](#)
14. Ma, Q.; Jin, H.; Zhu, J.; Li, Z.; Xu, H.; Liu, B.; Zhang, Z.; Ma, J.; Mu, S. Stabilizing Fe-N-C catalysts as model for oxygen reduction reaction. *Adv. Sci.* **2021**, *8*, 2102209. [\[CrossRef\]](#)
15. Li, Z.; Fang, Y.; Zhang, J.; Lou, X.W. Necklace-like structures composed of Fe₃N@c yolk-shell particles as an advanced anode for sodium-ion batteries. *Adv. Mater.* **2018**, *30*, 1800525. [\[CrossRef\]](#)

16. Zheng, Y.; He, F.; Wu, J.; Ma, D.; Fan, H.; Zhu, S.; Li, X.; Lu, Y.; Liu, Q.; Hu, X. Nitrogen-doped carbon nanotube–graphene frameworks with encapsulated Fe/Fe₃N nanoparticles as catalysts for oxygen reduction. *ACS Appl. Nano Mater.* **2019**, *2*, 3538–3547. [[CrossRef](#)]
17. Chen, Y.; Li, Z.; Zhu, Y.; Sun, D.; Liu, X.; Xu, L.; Tang, Y. Atomic Fe dispersed on N-doped carbon hollow nanospheres for high-efficiency electrocatalytic oxygen reduction. *Adv. Mater.* **2019**, *31*, 1806312. [[CrossRef](#)] [[PubMed](#)]
18. Yin, H.; Zhang, C.; Liu, F.; Hou, Y. Hybrid of iron nitride and nitrogen-doped graphene aerogel as synergistic catalyst for oxygen reduction reaction. *Adv. Funct. Mater.* **2014**, *24*, 2930–2937. [[CrossRef](#)]
19. Kosłowski, U.I.; Abs-Wurmbach, I.; Fiechter, S.; Bogdanoff, P. Nature of the catalytic centers of porphyrin-based electrocatalysts for the ORR: A correlation of kinetic current density with the site density of Fe–N₄ centers. *J. Phys. Chem. C* **2008**, *112*, 15356–15366. [[CrossRef](#)]
20. Zhou, L.; Li, Y.; Chen, X.; Yang, Z.; Yang, S.; Wang, Q.; Liu, X.-Y.; Lu, S. New insights into degradation of Fe–N–C catalyst layers: Ionomer decomposition. *J. Mater. Chem. A* **2022**, *10*, 20323–20330. [[CrossRef](#)]
21. Hu, Y.; Huang, D.; Zhang, J.; Huang, Y.; Balogun, M.-S.J.T.; Tong, Y. Dual doping induced interfacial engineering of Fe₂N/Fe₃N hybrids with favorable d-band towards efficient overall water splitting. *ChemCatChem* **2019**, *11*, 6051–6060. [[CrossRef](#)]
22. Chen, Z.Y.; Li, Y.N.; Lei, L.L.; Bao, S.J.; Wang, M.Q.; Heng, L.; Zhao, Z.L.; Xu, M.W. Investigation of Fe₂N@carbon encapsulated in N-doped graphene-like carbon as a catalyst in sustainable zinc–air batteries. *Catal. Sci. Technol.* **2017**, *7*, 5670–5676. [[CrossRef](#)]
23. Zhang, N.; Xie, S.; Wang, W.; Xie, D.; Zhu, D.; Cheng, F. Ultra-small Fe₂N/N-cnts as efficient bifunctional catalysts for rechargeable Zn–air batteries. *J. Electrochem. Soc.* **2020**, *167*, 020505. [[CrossRef](#)]
24. Compagnini, G.; Puglisi, O.; Foti, G. Raman spectra of virgin and damaged graphite edge planes. *Carbon* **1997**, *35*, 1793–1797. [[CrossRef](#)]
25. Li, L.; Qing, M.; Liu, X.; Wang, H.; Liu, S.; Zhang, Y.; Wan, H.; Wen, X.; Yang, Y.; Li, Y. Efficient one-pot synthesis of higher alcohols from syngas catalyzed by iron nitrides. *ChemCatChem* **2020**, *12*, 1939–1943. [[CrossRef](#)]
26. Zhu, C.; Fu, S.; Song, J.; Shi, Q.; Su, D.; Engelhard, M.H.; Li, X.; Xiao, D.; Li, D.; Estevez, L.; et al. Self-assembled Fe–N-doped carbon nanotube aerogels with single-atom catalyst feature as high-efficiency oxygen reduction electrocatalysts. *Small* **2017**, *13*, 1603407. [[CrossRef](#)]
27. Du, P.; Bao, Y.; Guo, C.; Wu, L.; Pan, J.; Zhao, C.; Ma, F.-X.; Lu, J.; Li, Y.Y. Design of Fe,N Co-doped multi-walled carbon nanotubes for efficient oxygen reduction. *Chem. Commun.* **2020**, *56*, 14467–14470. [[CrossRef](#)]
28. Zhu, G.; Ma, L.; Lv, H.; Hu, Y.; Chen, T.; Chen, R.; Liang, J.; Wang, X.; Wang, Y.; Yan, C.; et al. Pine needle-derived microporous nitrogen-doped carbon frameworks exhibit high performances in electrocatalytic hydrogen evolution reaction and supercapacitors. *Nanoscale* **2017**, *9*, 1237–1243. [[CrossRef](#)]
29. Guo, C.; Li, L.; Zhang, T.; Xu, Y.; Huo, Y.; Li, S. Space-confined iron nanoparticles in a 3D nitrogen-doped rgo-cnt framework as efficient bifunctional electrocatalysts for rechargeable zinc–air batteries. *Microporous Mesoporous Mater.* **2020**, *298*, 110100. [[CrossRef](#)]
30. Liu, S.; Zheng, W.; Xie, W.; Cui, H.; Li, Y.; Zhang, C.; Ji, Z.; Liu, F.; Chen, R.; Sun, H.; et al. Synthesis of three-dimensional honeycomb-like Fe₃N@nc composites with enhanced lithium storage properties. *Carbon* **2022**, *192*, 162–169. [[CrossRef](#)]
31. Qi, Y.; Li, Q.-J.; Wu, Y.; Bao, S.-J.; Li, C.; Chen, Y.; Wang, G.; Xu, M. A Fe₃N/carbon composite electrocatalyst for effective polysulfides regulation in room-temperature Na–S batteries. *Nat. Commun.* **2021**, *12*, 6347. [[CrossRef](#)] [[PubMed](#)]
32. Ma, J.; Li, J.; Wang, R.; Yang, Y.; Yin, P.; Mao, J.; Ling, T.; Qiao, S. Hierarchical porous S-doped Fe–N–C electrocatalyst for high-power-density zinc–air battery. *Mater. Today Energy* **2021**, *19*, 100624. [[CrossRef](#)]
33. Zhou, X.; Gao, J.; Hu, Y.; Jin, Z.; Hu, K.; Reddy, K.M.; Yuan, Q.; Lin, X.; Qiu, H.-J. Theoretically revealed and experimentally demonstrated synergistic electronic interaction of CoFe dual-metal sites on N-doped carbon for boosting both oxygen reduction and evolution reactions. *Nano Lett.* **2022**, *22*, 3392–3399. [[CrossRef](#)] [[PubMed](#)]
34. Wang, B.; Tang, J.; Zhang, X.; Hong, M.; Yang, H.; Guo, X.; Xue, S.; Du, C.; Liu, Z.; Chen, J. Nitrogen doped porous carbon polyhedral supported Fe and Ni dual-metal single-atomic catalysts: Template-free and metal ligand-free synthesis with microwave-assistance and d-band center modulating for boosted ORR catalysis in zinc–air batteries. *Chem. Eng. J.* **2022**, *437*, 135295. [[CrossRef](#)]
35. Ye, H.; Li, L.; Liu, D.; Fu, Q.; Zhang, F.; Dai, P.; Gu, X.; Zhao, X. Sustained-release method for the directed synthesis of ZIF-derived ultrafine Co–N–C ORR catalysts with embedded Co quantum dots. *ACS Appl. Mater. Interfaces* **2020**, *12*, 57847–57858. [[CrossRef](#)]
36. Hu, C.; Dai, L. Carbon-based metal-free catalysts for electrocatalysis beyond the ORR. *Angew. Chem. Int. Ed.* **2016**, *55*, 11736–11758. [[CrossRef](#)]
37. Zhang, J.; Wang, M.; Wan, T.; Shi, H.; Lv, A.; Xiao, W.; Jiao, S. Novel (Pt–O(x))–(Co–O(y)) nonbonding active structures on defective carbon from oxygen-rich coal tar pitch for efficient HER and ORR. *Adv. Mater.* **2022**, *34*, e2206960. [[CrossRef](#)]

Disclaimer/Publisher’s Note: The statements, opinions and data contained in all publications are solely those of the individual author(s) and contributor(s) and not of MDPI and/or the editor(s). MDPI and/or the editor(s) disclaim responsibility for any injury to people or property resulting from any ideas, methods, instructions or products referred to in the content.